Hindawi
Mathematical Problems in Engineering
Volume 2024, Article ID 3359266, 15 pages
https://doi.org/10.1155/2024/3359266

Research Article

A Study on the Vehicle Antilock System Based on Adaptive Neural Network Sliding Mode Control

Yaoping Li and Han Li

Faculty of Transportation Engineering, Kunming University of Science and Technology, Kunming 650500, China

Correspondence should be addressed to Yaoping Li; 20050136@kust.edu.cn

Received 22 October 2023; Revised 21 February 2024; Accepted 27 February 2024; Published 11 March 2024

Academic Editor: Francisco Rossomando

Vehicle antilock systems play a very important role in the stability and reliability during vehicle braking. Due to the complexity of the braking process, antilock braking system (ABS) usually face the problems such as nonlinearity, time-varying, and uncertain parameter modeling. Thus, aiming at the parameter model uncertainty problem of ABS, an adaptive neural network sliding mode controller (ADRBF-SMC) is designed in this paper. On this basis, establishing the quarter-vehicle model and the seven-degree-of-freedom vehicle model, and treating the difference between the two models as a kind of disturbance, carrying out vehicle braking performance simulation experiments to analyze the variation of braking performance parameters such as vehicle and wheel speeds, slip ratio, braking distance, braking torque, under the three cases of adaptive neural network sliding mode controller, traditional sliding mode controller, and no control. Simulation results show that the adaptive neural network sliding mode controller (ADRBF-SMC) proposed in this paper can play an effective control role in both vehicle dynamics models. In addition, the control method proposed in this paper has stronger anti-interference capability and higher robustness compared with the sliding mode controller (SMC).

1. Introduction

In the past decades, vehicle active safety devices have been not only an important guarantee of vehicle driving safety but also a hot issue of concern for researchers and vehicle manufacturers. Antilock braking system (ABS) is a key and essential vehicle active safety device. ABS is able to make the vehicle wheels in the state of rolling and sliding in the event of an emergency braking to keep the vehicle tires in contact with the ground to generate maximum ground braking force to prevent the wheels from locking up and causing the vehicle to lose steering ability, which reduces traffic and protects the safety of vehicle occupants. The key to the maximum braking force achieved by ABS is the control of the wheel slip ratio of the vehicle. Vehicles in the face of different road surfaces, different tires, always exist within a certain range so that the tires get the best adhesion slip ratio. Control slip ratio in a certain range can realize the best adhesion, and then produce the best braking force, so as to realize the purpose of ABS.

In past studies, researchers have used various mainstream control methods such as proportional–integral–derivative (PID), fuzzy control, sliding mode control, optimal control, adaptive control, self-adaptive control, self-resistant control, model predictive control, state observers, and neural networks in order to solve the uncertainty problem and to realize the function of ABS in order to achieve the slip ratio control objective. Most of the scholars study the slip ratio control process with in-depth control algorithms based on the vehicle quarter model or called single wheel model.

Moaaz et al. [1] verified the ABS performance of PID control on a single-wheel model. He et al. [2], with a single-wheel model, proposed a model predictive control method for estimating the optimal slip ratio of an electric motor ABS for pure electric vehicles. The designed estimation method and the obtained MPC law are embedded into the vehicle control unit (VCU) for real vehicle validation. Li et al. [3] illustrated the feasibility of controlling ABS with self-resilience by considering a single-wheel model. Wang et al. [4] designed a constrained control method based on tangential barrier Lyapunov function (Tan-BLF) considering a quarter-vehicle braking model with uncertainty. Constrain the slip ratio of the ABS to the stabilization region at all times as well [5]. An improved global sliding mode control scheme was proposed to further improve the braking performance of nonlinear ABS using a quarter-vehicle model. This method eliminates the arrival phases compared to the conventional sliding mode control and ensures the robustness of the system throughout the control process. García Torres et al. [6], among others, simulated a quarter car model to design an improved higher order sliding mode controller based on PID control, which was applied to an ABS laboratory unit to track the appropriate slip ratio values, which resulted in a considerable increase in the efficiency of the control system as compared to the PID-like controller. Zhang et al. [7] proposed switching the motor torque control between gap sliding mode compensation and elastic double closed-loop PID compensation to significantly improve the antilock braking comfort, stability, and maneuverability of an electric vehicle based on the antilock braking wheel slip ratio objective on the left front wheel of a quarter car. Feng and Hu [8] designed a discrete fuzzy adaptive PID control algorithm for automotive ABS with a single-wheel model of the vehicle to solve the problems of low skidding rate and poor braking performance of automotive ABS. Amirkhani et al. [9] constructed an indirect exponential sliding mode controller based on interval type-2 fuzzy neural network using a quarter-vehicle model in order to improve the performance of vehicle antilock braking system in the face of uncertainty [10]. Considering a quarter-vehicle model, in order to control the wheel slip ratio at an optimal value, the effective parameters of the wheels that affect the dynamic performance and stability of the vehicle during braking and steering inputs are investigated using an intelligent adaptive fuzzy controller capable of estimating the parameters online. Zhang et al. [11] established a quarter-vehicle model with wheel angular velocity and vehicle longitudinal velocity as states, proposed a robust adaptive wheel slip ratio tracking control method with state observer, and verified the effectiveness and feasibility of the proposed method based on a model-in-the-loop simulation system. Ben Moussa and Bakhti [12] evaluated the robustness of adaptive model predictive controller and first-order sliding mode controller (FOSMC) on a quarter-vehicle model in tracking the longitudinal slip ratio of tires in the face of modeling uncertainties or external disturbances. Both were found to ensure perfect tracking of tire longitudinal slip ratio setpoints by the ABS, but the FOSMC-based ABS was unable to maintain near-nominal braking performance at road inclines, with very slow braking times at higher angles. The use of another type of sliding mode control can compensate for the limitations obtained by sliding first-order modes, in particular by using higher order sliding modes. Zhang et al. [13], developed a quarter-vehicle aggregate uncertainty wheel slip ratio dynamics model used RBFNN with unknown optimal weight vectors adaptively adjusted to approximate and compensate for the aggregate uncertainty, and designed a new tracking differentiator to compute the derivatives of the desired wheel slip ratio, and the proposed control strategy is able to track the desired wheel slip ratio quickly and accurately. Hsu [14] proposed an intelligent exponential sliding mode control system based on a quarter-vehicle model, designed a function recursive fuzzy neural network uncertainty estimator to approximate the unknown nonlinear term of the ABS dynamics, and derived the parameter adaptive law in the sense of projection algorithms and Lyapunov's stability theorem, which ensured the stable control performance of ABS. Chereji et al. [15] simulated the relative motion between the road (lower wheels) and the quarter car model (upper wheels), presented the performance of two sliding mode control algorithms based on Lyapunov's sliding mode controller and law of arrival-based sliding mode controller, and updated the design and applied it to the ABS.

The quarter model of the vehicle has a simple structure and to some extent is also able to represent wheel dynamics and well represent the slip rate control strategy. The reason used by research scholars is to ignore the complexity of the model and the research focuses on the control algorithms, and this line of thinking has some effect. But the slip ratio is controlled to improve ABS performance, and ABS always runs the entire vehicle. The differences that exist between the vehicle quarter model and the full vehicle model are not conducive to real vehicle operation. So in order to study the designed controller in depth, the researchers built half-vehicle and full-vehicle models by considering the model and control algorithm together. On a semivehicle model, Radac and Precup [16], on a two-wheeled experimental setup, proposed the design and implementation of a reinforcement Q-learning optimal control method incorporating neural networks for model-free tire skidding control method against a fast, highly nonlinear ABS. Wang and He [17] proposed an improved optimal slip mode controller with a vehicle longitudinal half-vehicle dynamics model not only has strong robustness to the uncertainty of the roadway attachment coefficient but also has a better control performance of the slip ratio. The researchers use the full vehicle model to study ABS and further restore the actual use of ABS. Lv et al. [18] developed an electrohydraulic composite ABS and its corresponding braking torque distribution strategy for electric vehicles based on interval type-2 fuzzy logic control strategy with a seven-degree-of-freedom whole-vehicle dynamics model, obtaining a better slip ratio control effect and excellent robustness. Fu [19] proposed a variable domain fuzzy PID control strategy based on particle swarm optimization algorithm on a seven-degree-of-freedom vehicle model to safeguard the braking effect of automotive ABS. Sun et al. [20] introduced a four-wheel ABS based on fuzzy sliding mode control, and the control performance was verified by multiple braking simulations and joint simulations under complex road conditions [21]. The improved adaptive sliding mode controller realized the effective control of the optimal slip ratio by taking distributed drive electric vehicle as the research object, and the studied control method can effectively estimate and control the optimal slip rate under various complex road surfaces. He et al. [22] in order to improve the braking stability of pure electric vehicles, a combined sliding mode control method for electric motor antilock braking system (emABS) was proposed by designing the emABS control law using two key variables, wheel deceleration and slip ratio. Soltani et al. [23] proposed an adaptive neuro-fuzzy inference system to obtain the optimal tire slip rate on a seven-degree-of-freedom vehicle model in response to the fact that the performance of ABS for shortening the braking distance depends on the optimal tire slip ratio. Sun et al. [24] developed a four-wheel model of a vehicle that includes wheel resistance and air resistance and proposed a slip-model wheel slip ratio controller to realize antilock control of wheels with adaptive sliding surfaces. It ensures that the vehicle does not skid during braking and reduces stopping distances under certain road conditions.

Many scholars study ABS primarily with quarter models, which focus on the control method. The vehicle quarter model has a simple structure and can verify the effectiveness of the control algorithm. However, due to the consideration of too few factors, it is not able to demonstrate the effectiveness of the proposed control algorithm in solving the uncertainty problem of ABS. Compared with the quarter-vehicle model, the whole-vehicle model considers more vehicle parameters [25], which is more convincing in restoring the actual use environment of ABS and verifying the effectiveness of the proposed control method. Sliding mode control is a common control method in vehicle control problems. When the state trajectory reaches the sliding mode surface, it is difficult to slide strictly along the sliding mode surface toward the equilibrium point, and vibration will be generated when using this control method for ABS control.

Therefore, this paper establishes a vehicle quarter model and a seven-degree-of-freedom vehicle model. The difference between the two models is treated as a disturbance term. The slip mode control is proposed based on the slip ratio of ABS, and the adaptive neural network control is proposed on the basis of the slip mode control to further optimize the slip mode control. On this basis, the simulation analysis is carried out and the variations of the parameters such as vehicle speed and wheel speed, wheel braking torque, braking distance as well as slip ratio of ABS under sliding mode control, adaptive neural network sliding mode control, and no control are obtained. The final results show that the proposed control method can be effectively used for ABS slip ratio control and ABS modeling uncertainty problem solving.

The main content of the paper includes the establishment of a quarter-vehicle dynamics model and a whole vehicle seven-degree-of-freedom dynamics model that includes the vehicle longitudinal, lateral, yaw, and four wheels. Based on the ABS slip ratio control theory, the adaptive neural network slip mode control method is proposed to track the ideal slip ratio by treating the uncertainty of the model with neural network and adaptive rate. Finally, based on the two models, simulation analysis was carried out in three cases: adaptive neural network sliding mode controller, sliding mode controller, and no control. The main contributions of the paper are as follows: (a) Based on the quarter-vehicle model and the seven-degree-of-freedom whole-vehicle model, the adaptive neural network sliding mode control method is proposed by considering the influence of ABS modeling uncertainty on the slip ratio control algorithm and (b) the proposed control method realizes the control of ABS slip ratio effectively. Moreover, compared with the sliding mode control, the proposed adaptive neural network sliding mode control method carries out the control with less jitter.

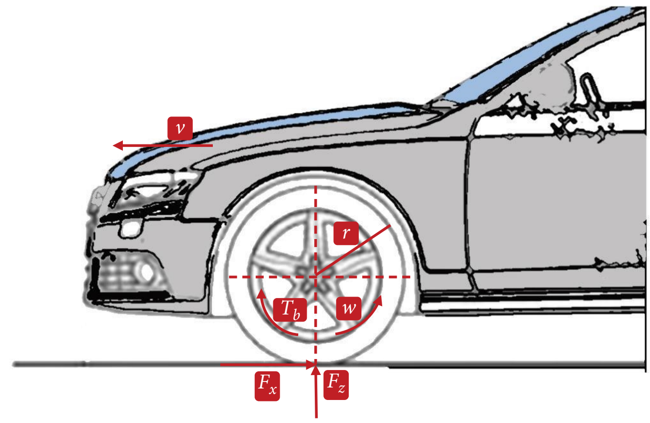

Figure 1: Schematic of quarter car model.

2. Mathematical Modeling of Antilock Braking Systems

2.1. Quarter-Vehicle Dynamics Model. ABS of the quarter-vehicle model is shown in Figure 1.

The model consists of a quarter-vehicle mass is $m_c/4$ and a single wheel mass is m_w. The speed at which the vehicle is traveling is v, the angular velocity of the wheels is w, the rolling radius of the wheels is r, the brake moment of the wheels is T_b, the moment of inertia of the wheels is I_w, the tangential reaction force between the wheels and the ground is F_x, and the ground normal force is F_z.

The dynamic equations of the wheel can be obtained by the following equations:

$$m\dot{v} = -F_x, \tag{1}$$

$$I_w\dot{w} = F_x r - T_b, \tag{2}$$

$$F_x = \mu F_z, \tag{3}$$

where μ is the ground adhesion coefficient and $m = 1/4m_c + m_w$ is the sum of the mass of the quarter body and the mass of the individual wheels.

The tire model of the vehicle quarter dynamics model uses Burckhardt's [26] study who gave a commonly used kind of functional relationship between the longitudinal attachment coefficient μ of the tire and the slip ratio λ:

$$\mu(\lambda) = C_1\left(1 - e^{-C_2\lambda}\right) - C_3\lambda, \tag{4}$$

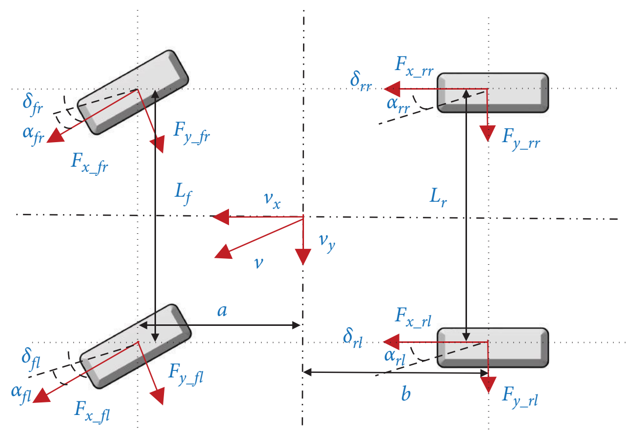

FIGURE 2: Vehicle dynamics model.

where C_1, C_2, C_3 are pavement fitting parameters, and common pavements are selected, then $C_1 = 1.281, C_2 = 23.93$, $C_3 = 0.52$.

The ratio of slip produced by the wheels against the ground while the vehicle is in motion is calculated by the following equation:

$$\lambda = \frac{v - wr}{v}. \tag{5}$$

Substituting Equations (1) and (2) into Equation (5) gives the following equation:

$$\dot{\lambda} = -\frac{1}{v}\left(\frac{F_x}{m}(1-\lambda) + \frac{r^2}{I_w}F_x\right) + \left(\frac{r}{I_w v_x}\right)T_b. \tag{6}$$

2.2. Vehicle Dynamics Model. The vehicle model can describe the motion characteristics of the vehicle, so the whole vehicle dynamics model with seven degrees of freedom is used in this paper [27]. The vehicle dynamics model is shown in Figure 2.

The seven-degree-of-freedom vehicle dynamics model includes longitudinal motion, lateral motion, yaw motion, and rotational motion of four wheels.

Longitudinal equations of motion for vehicles are as follows:

$$\begin{aligned} F_x = {} & F_{x\_fl}\cos\delta_{fl} - F_{y\_fl}\sin\delta_{fl} \\ & + F_{x\_fr}\cos\delta_{fr} - F_{y\_fr}\sin\delta_{fr} \\ & + F_{x\_rl}\cos\delta_{rl} - F_{y\_rl}\sin\delta_{rl} \\ & + F_{x\_rr}\cos\delta_{rr} - F_{y\_rr}\sin\delta_{rr}, \end{aligned} \tag{7}$$

$$\begin{aligned} ma_x = {} & F_x - m_s h_s \dot{\beta} w_r - mgf \\ & - v_x^2 \cdot 0.5(A\rho C_d), \end{aligned} \tag{8}$$

$$a_x = \dot{v}_x - v_y w_r, \tag{9}$$

where $F_{x\_fl}, F_{x\_fr}, F_{x\_rl}, F_{x\_rr}$ are the longitudinal forces between the four wheels and the ground. $F_{y\_fl}, F_{y\_fr}, F_{y\_rl}$, F_{y_rr} are the lateral forces between the four wheels and the ground, respectively. $\delta_{fl}, \delta_{fr}, \delta_{rl}, \delta_{rr}$ are the steering angles of the four wheels. w_r is the transverse angular velocity. β is the vehicle lateral camber. a_x is the vehicle longitudinal acceleration.

The lateral equations of motion of a vehicle are as follows:

$$\begin{aligned} F_y = {} & F_{x\_fl}\sin\delta_{fl} + F_{y\_fl}\cos\delta_{fl} \\ & + F_{x\_fr}\sin\delta_{fr} + F_{y\_fr}\cos\delta_{fr} \\ & + F_{x\_rl}\sin\delta_{rl} + F_{y\_rl}\cos\delta_{rl} \\ & + F_{x\_rr}\sin\delta_{rr} + F_{y\_rr}\cos\delta_{rr}, \end{aligned} \tag{10}$$

$$ma_y = F_y + m_s h_s \ddot{\beta}, \tag{11}$$

$$\dot{v}_y + v_x w_r = a_y. \tag{12}$$

The equations of motion for the yaw motion of the vehicle are as follows:

$$\begin{aligned} M = {} & a\left(F_{x\_fl}\sin\delta_{fl} + F_{y\_fl}\cos\delta_{fl} + F_{x\_fr}\sin\delta_{fr} + F_{y\_fr}\cos\delta_{fr}\right) \\ & - b\left(F_{x\_rl}\sin\delta_{rl} + F_{y\_rl}\cos\delta_{rl} + F_{x\_rr}\sin\delta_{rr} + F_{y\_rr}\cos\delta_{rr}\right) \\ & - \frac{L_f}{2}\left(F_{x\_fl}\cos\delta_{fl} - F_{y\_fl}\sin\delta_{fl} - F_{x\_fr}\cos\delta_{fr} + F_{y\_fr}\sin\delta_{fr}\right) \\ & - \frac{L_r}{2}\left(F_{x\_rl}\cos\delta_{rl} - F_{y\_rl}\sin\delta_{rl} - F_{x\_rr}\cos\delta_{rr} + F_{y\_rr}\sin\delta_{rr}\right), \end{aligned} \tag{13}$$

$$I_z \dot{w}_r = M + \ddot{\beta} I_{xz}, \tag{14}$$

where a and b are the distances from the center of mass to the front and rear axles of the vehicle, respectively. L_f and L_r are the wheelbase between the front and rear wheels of the vehicle, respectively. I_{xz} is the mass moment of inertia of the spring-loaded mass. I_z is the moment of inertia of the vehicle around the z-axis.

In order to describe the vehicle dynamics in a better way, this paper adopts the Magic Formula (MF) tire model, which is widely used due to its high fitting accuracy.

The equation for the MF model is as follows:

$$R\ \sin\{S\arctan[Ts - W(Ts - \arctan(Ts))]\} = F_{x\_ij}, \tag{15}$$

where F_{x_ij} represents the four wheels.

The center speed of the wheel is calculated by the following equation:

$$\begin{aligned} \left(v_x - 0.5L_f w_r\right)\cos\delta_{fl} + \left(v_y + aw_r\right)\sin\delta_{fl} &= v_{fl} \\ \left(v_x + 0.5L_f w_r\right)\cos\delta_{fr} + \left(v_y + aw_r\right)\sin\delta_{fr} &= v_{fr} \\ \left(v_x - 0.5L_r w_r\right)\cos\delta_{rl} + \left(v_y - bw_r\right)\sin\delta_{rl} &= v_{rl} \\ \left(v_x + 0.5L_r w_r\right)\cos\delta_{rr} + \left(v_y - bw_r\right)\sin\delta_{rr} &= v_{rr}, \end{aligned} \tag{16}$$

where v_{fl}, v_{fr}, v_{rl}, and v_{rr} represent the tire center speeds of the left front wheel, right front wheel, left rear wheel, and right rear wheel, respectively.

Tire side deflection angle is as follows:

$$\begin{aligned}&\arctan\left(\frac{v_y+aw_r}{v_x-0.5L_f w_r}\right)-\delta_{fl}=\alpha_{fl}\\&\arctan\left(\frac{v_y+aw_r}{v_x+0.5L_f w_r}\right)-\delta_{fr}=\alpha_{fr}\\&\arctan\left(\frac{v_y-aw_r}{v_x-0.5L_r w_r}\right)-\delta_{rl}=\alpha_{rl}\\&\arctan\left(\frac{v_y-a\cdot w_r}{v_x+0.5L_r\cdot w_r}\right)-\delta_{rr}=\alpha_{rr}.\end{aligned} \tag{17}$$

Vertical loads on the wheels are as follows:

$$\begin{aligned}&\frac{mgb}{2L}-\frac{ma_xh}{2L}-\frac{ma_yhb}{L_fL}=F_{z\_fl},\frac{mgb}{2L}-\frac{ma_xh}{2L}+\frac{ma_yhb}{L_fL}=F_{z\_fr}\\&\frac{mga}{2L}+\frac{ma_xh}{2L}-\frac{ma_yha}{L_fL}=F_{z\_rl},\frac{mga}{2L}+\frac{ma_xh}{2L}+\frac{ma_yha}{L_fL}=F_{z\_rr},\end{aligned} \tag{18}$$

where $F_{z\_fl}, F_{z\_fr}, F_{z\_rl}$, and F_{z_rr} represent the vertical loads on the left front wheel, right front wheel, left rear wheel, and right rear wheel, respectively.

Wheel dynamics equations are as follows:

$$\begin{aligned}&F_{x\_fl}r-T_{b\_fl}=I_w\dot{w}_{fl},F_{x\_fr}r-T_{b\_fr}=I_w\dot{w}_{fr}\\&F_{x\_rl}r-T_{b\_rl}=I_w\dot{w}_{rl},F_{x\_rr}r-T_{b\_rr}=I_w\dot{w}_{rr},\end{aligned} \tag{19}$$

where $T_{b\_fl}, T_{b\_fr}, T_{b\_rl}$, and T_{b_rr} represent the brake moments of the left front, right front, left rear, and right rear wheels, respectively. w_{fl}, w_{fr}, w_{rl}, and w_{rr} represent the angular velocities of the left front wheel, right front wheel, left rear wheel, and right rear wheel, respectively.

Wheel slip ratio is as follows:

$$\begin{aligned}&\frac{v_{x\_fl}-w_{fl}r}{v_{x\_fl}}=\lambda_{fl},\frac{v_{x\_fr}-w_{fr}r}{v_{x\_fr}}=\lambda_{fr}\\&\frac{v_{x\_rl}-w_{rl}r}{v_{x\_rl}}=\lambda_{rl},\frac{v_{x\_rr}-w_{rr}r}{v_{x\_rr}}=\lambda_{rr},\end{aligned} \tag{20}$$

where $\lambda_{fl}, \lambda_{fr}, \lambda_{rl}$, and λ_{rr} represent the slip ratios of the left front wheel, right front wheel, left rear wheel, and right rear wheel, respectively.

3. Control Structure of the ABS

3.1. Sliding Mode Control. Sliding mode control has the property of finite convergence for highly nonlinear systems and good robustness to changes [28]. So it is suitable for solving the problem of slip ratio control in ABS. The control of slip ratio is usually done by keeping the slip ratio of the wheel at the slip ratio corresponding to the maximum ground adhesion coefficient as the ideal slip ratio λ_d.

Assuming that the optimal slip ratio corresponding to the maximum tire force between the wheel and the ground is 0.2. In order to include the transient response of the reference model of the wheel slip ratio and to prevent large tracking errors and consequent large control capacity of the wheel at the onset of braking, the following system is regarded as an ideal model of wheel slip [29]:

$$\lambda_d=\frac{\lambda'}{s}\frac{\varepsilon}{s+\varepsilon}, \tag{21}$$

where ε is the time constant taking the value of 20.

Laplace inverse transformation is done on both sides of the equation to solve the first-order differential equation with zero initial condition:

$$\lambda_d(t)=\lambda'-\lambda' e^{-\varepsilon t}. \tag{22}$$

Define the tracking error of the controller:

$$e=\lambda-\lambda_d. \tag{23}$$

The switching function for sliding mode variable structure control is selected:

$$s=e+k_1\int_0^t e(t)dt, \tag{24}$$

where k_1 is a constant greater than zero. t is the time.

Derive Equation (23) and substitute into Equation (24) in the differentiation of the switching function, we get the following equation:

$$\dot{s}=\dot{e}+k_1e=\dot{\lambda}-\dot{\lambda}_d+k_1e. \tag{25}$$

Substituting Equation (6) into Equation (25) gives the following equation:

$$\dot{s}=-\frac{1}{v}\left(\frac{F_x}{m}(1-\lambda)+\frac{r^2}{I_w}F_x\right)+\left(\frac{r}{I_wv_x}\right)T_b-\dot{\lambda}_d+k_1e. \tag{26}$$

The sliding mode control uses an exponential convergence rate and the design switching function is obtained:

$$\dot{s}=-k_2\,\mathrm{sgn}(s)-k_3s, \tag{27}$$

where k_2 is the switching term gain, k_3 is the power convergence term coefficient, $k_2>0, k_3>0$. $\mathrm{sgn}(s)$ is the sign function.

Associative Equations (26) and (27) are obtained as follows:

$$\begin{aligned}T_b=&\frac{I_wv_x}{r}\frac{1}{v}\left(\frac{F_x}{m}(1-\lambda)+\frac{r^2}{I_w}F_x\right)\\&+\dot{\lambda}_d-k_1e+k_2\,\mathrm{sgn}(s)+k_3s.\end{aligned} \tag{28}$$

In order to try to eliminate the effect of sliding mode control jitter and make the switching function continuous, a saturation function is used to replace the sign function $\mathrm{sgn}(s)$, and the saturation function $\mathrm{sat}(s)$ is as follows:

$$\mathrm{sat}(s) = \begin{cases} \mathrm{sgn}(s), & |s| > \Delta \\ \dfrac{s}{\Delta}, & |s| \le \Delta \end{cases}, \tag{29}$$

where Δ takes the value of a constant greater than zero.

Then the sliding mode control rate after the saturation function treatment is as follows:

$$\begin{aligned} T_b = & \frac{I_w v_x}{r}\frac{1}{v}\left(\frac{F_x}{m}(1-\lambda) + \frac{r^2}{I_w}F_x\right) \\ & + \dot{\lambda}_d - k_1 e + k_2 \mathrm{sat}(s) + k_3 s. \end{aligned} \tag{30}$$

Define the Lyapunov function as:

$$V_1 = \frac{1}{2}s^2. \tag{31}$$

Derivation of Equation (31) and substitution of Equations (27) and (29) gives the following equation:

$$\begin{aligned} \dot{V}_1 &= s\dot{s} = s(-k_2 \mathrm{sat}(s) - k_3 s) \\ &= -k_2 s \cdot \mathrm{sat}(s) - k_3 s^2, \end{aligned} \tag{32}$$

where since $s \cdot \mathrm{sat}(s) > 0$, then $\dot{V}_1 \le 0$. The system is asymptotically stable according to Lyapunov's stability principle. Then, when the ABS controller satisfies the control rate shown in Equation (30), the ABS is stable and vice versa.

3.2. Adaptive Neural Network Sliding Mode Control. From Equation (6), the system can be normalized as follows:

$$\dot{\lambda} = f(x) + g(x)u, \tag{33}$$

where $\boldsymbol{X} = [x_1 \quad x_2]^T = [v \quad \lambda]^T$ is the state vector and T_b is the control input. $f(\boldsymbol{X}) = -(F_x(1-\lambda)/m + r^2 F_x/I_w)/v$, $g(\boldsymbol{X}) = r/I_w v_x$, $u = T_b$.

It is assumed that all the parameters of the vehicle during traveling are known and explicit, the developed nominal model of the system of Equation (33) can be expressed as follows:

$$\dot{\lambda} = f'(\boldsymbol{X}) + g'(\boldsymbol{X})u, \tag{34}$$

where f' and g' are the nominal values of f and g, respectively.

The system model built in the real situation deviates from the nominal model, here the deviation mainly comes from the constructed system model itself uncertainty, such as nonlinear dynamics, parameter variations, and perturbations. In order to deal with this kind of deviation and to improve the robustness of the system, the system described by Equation (33) is optimized as follows:

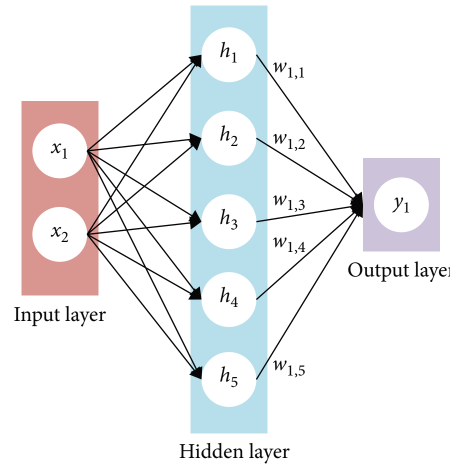

Figure 3: Schematic diagram of neural network structure.

$$\begin{aligned} \dot{\lambda} &= [f'(\boldsymbol{X}) + \Delta f(\boldsymbol{X})] \\ &\quad + [g'(\boldsymbol{X}) + \Delta g(\boldsymbol{X})]u \\ &= f'(\boldsymbol{X}) + g'(\boldsymbol{X})u + d, \end{aligned} \tag{35}$$

where $\Delta f(x)$ and $\Delta g(x)$ denote unknown uncertainties. d as a complementary term denotes the total set uncertainty, $d = \Delta f(\boldsymbol{X}) + \Delta g(\boldsymbol{X})u$, and there are restrictions on the total set uncertainty, $d \le N$, N are positive constants.

In order to ensure the improvement and optimization of the control performance on the sliding mode control, it can be obtained from Equations (24) and (27):

$$\dot{s} = f'(\boldsymbol{X}) + g'(\boldsymbol{X})u + k_1 e - \dot{\lambda}_d + d. \tag{36}$$

Similarly, the control rate can be obtained from Equations (27), (29), and (32):

$$\begin{aligned} u = & \frac{-f'(\boldsymbol{X}) + \dot{\lambda}_d - k_1 e - k_2 \mathrm{sat}(\boldsymbol{X})}{g'(\boldsymbol{X})} \\ & - \frac{k_3 s + d}{g'(\boldsymbol{X})}. \end{aligned} \tag{37}$$

The control rate of Equation (37) has a centralized uncertainty d. In order to make the control model more accurate and increase the anti-interference ability, the centralized uncertainty d is processed by the adaptive method. The real centralized uncertainty d is predicted by using the RBF neural network [30] in order to reduce the various uncertainties suffered by the controller in the control process.

The neural network structure used is shown in Figure 3. Predict the centralized uncertainty d, achieve adaptive approximation of the centralized uncertainty [31], and the network algorithm is as follows:

$$\begin{cases} d = W_{\boldsymbol{i}}^{*T} h_j(x) + \theta \\ \hat{d} = \widehat{W}_i h_j(x) \end{cases}, \tag{38}$$

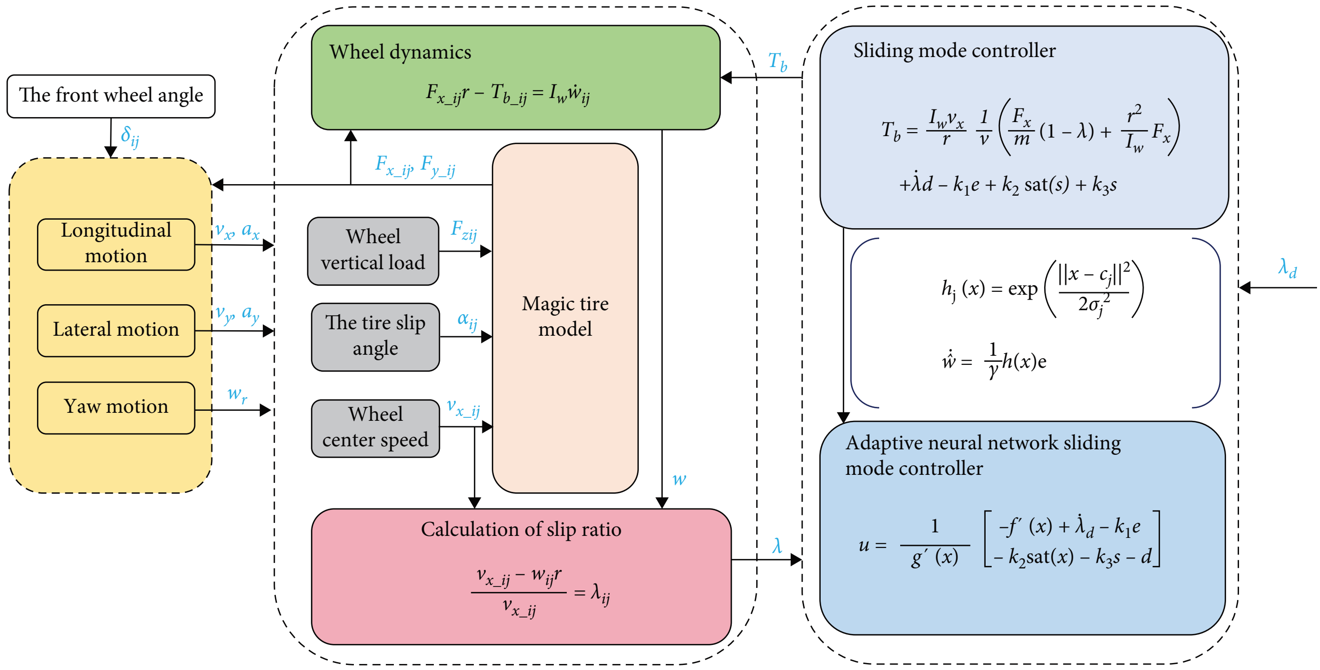

Figure 4: Schematic diagram of slip ratio control structure for adaptive neural network sliding mode controller (ADRBF-SMC).

Table 1: ABS vehicle quarter model parameters.

Description	Symbol	Value	Units
Quarter car mass	m_c	201.9	kg
Mass per wheel	m_w	98.1	kg
Wheel rolling radius	r	0.28	m
Wheel moment of inertia	I_w	3	Kg·m^2
Gravitational acceleration	g	9.8	m/s^2

where $\boldsymbol{W_i} = [W_1, \ldots, W_i]$ is the weights of the neural network, $i = 1, 2, \ldots, p$. $\boldsymbol{h_j}(x) = [h_1(x), \ldots, h_j(x)]$ is the output of the radial basis function, $j = 1, 2, \ldots, n$. θ is the approximation error of the network, $|\theta| \leq \theta_M$. $\widehat{\boldsymbol{W}}$ is an estimate of the network weights $\boldsymbol{W}^*$, $\tilde{\boldsymbol{W}} = \widehat{\boldsymbol{W}} - \boldsymbol{W}^*$. $\widehat{d}$ is an estimate of the total set uncertainty d.

A Gaussian function is chosen as the radial basis function for the hidden layer of the neural network:

$$h_j(x) = \exp\left(\frac{\|x - c_j\|^2}{2\sigma_j^2}\right), \tag{39}$$

where $\boldsymbol{x}$ represents the network input. $\boldsymbol{x} = [x_1 x_2 \ldots x_i]$ is the input vector of the neural network. σ_j is the normalization constant of the jth hidden node. j is the jth network input within the hidden layer of the network, $j = 1, 2, \ldots, n$, n is the number of hidden neurons. c_j is the center vector of the Gaussian function of the jth hidden node.

Combining Equations (37) and (38) gives the control rate:

$$u = \frac{-f'(\boldsymbol{X}) + \dot{\lambda}_d - k_1 e - k_2\mathrm{sat}(\boldsymbol{X})}{g'(\boldsymbol{X})} - \frac{k_3 s + \widehat{d}}{g'(\boldsymbol{X})}. \tag{40}$$

Define the Lyapunov function as follows:

$$V_2 = \frac{1}{2}e^2. \tag{41}$$

Combining Equations (23), (35), and (38) to derive Equation (41):

$$\dot{V}_2 = e\dot{e} = e\left[f'(\boldsymbol{X}) + g'(\boldsymbol{X})u + \boldsymbol{W}^{*T}\boldsymbol{h}(\boldsymbol{x}) + \theta - \dot{\lambda}_d\right]. \tag{42}$$

To make $\dot{V}_2 \leq 0$, assume that $\dot{V}_2 = -k_4 \cdot e^2$, then the following equation is obtained:

$$u = \frac{1}{g'(\boldsymbol{X})}\left[-f'(\boldsymbol{X}) - \widehat{\boldsymbol{W}}^T\boldsymbol{h}(\boldsymbol{x}) + \dot{\lambda}_d - k_4 e\right]. \tag{43}$$

Substituting Equation (43) into Equation (42) gives the following equation:

$$\begin{aligned}\dot{V}_2 &= e\left(-\widehat{\boldsymbol{W}}^T\boldsymbol{h}(\boldsymbol{x}) - k_4 e + \boldsymbol{W}^{*T}\boldsymbol{h}(\boldsymbol{x}) + \theta\right) \\ &= e\left(-\widetilde{\boldsymbol{W}}^T\boldsymbol{h}(\boldsymbol{x}) - k_4 e + \theta\right) = -k_4 e^2 - \widetilde{\boldsymbol{W}}^T\boldsymbol{h}(\boldsymbol{x})e + \theta e.\end{aligned} \tag{44}$$

Designing the update rate, a new Lyapunov function is considered due to the introduction of a new error variable $\tilde{W}$:

$$V_3 = V_2 + \frac{1}{2}\gamma\widetilde{\boldsymbol{W}}^T\widetilde{\boldsymbol{W}}, \tag{45}$$

where γ is the regulation parameter that regulates the update rate and is a positive constant.

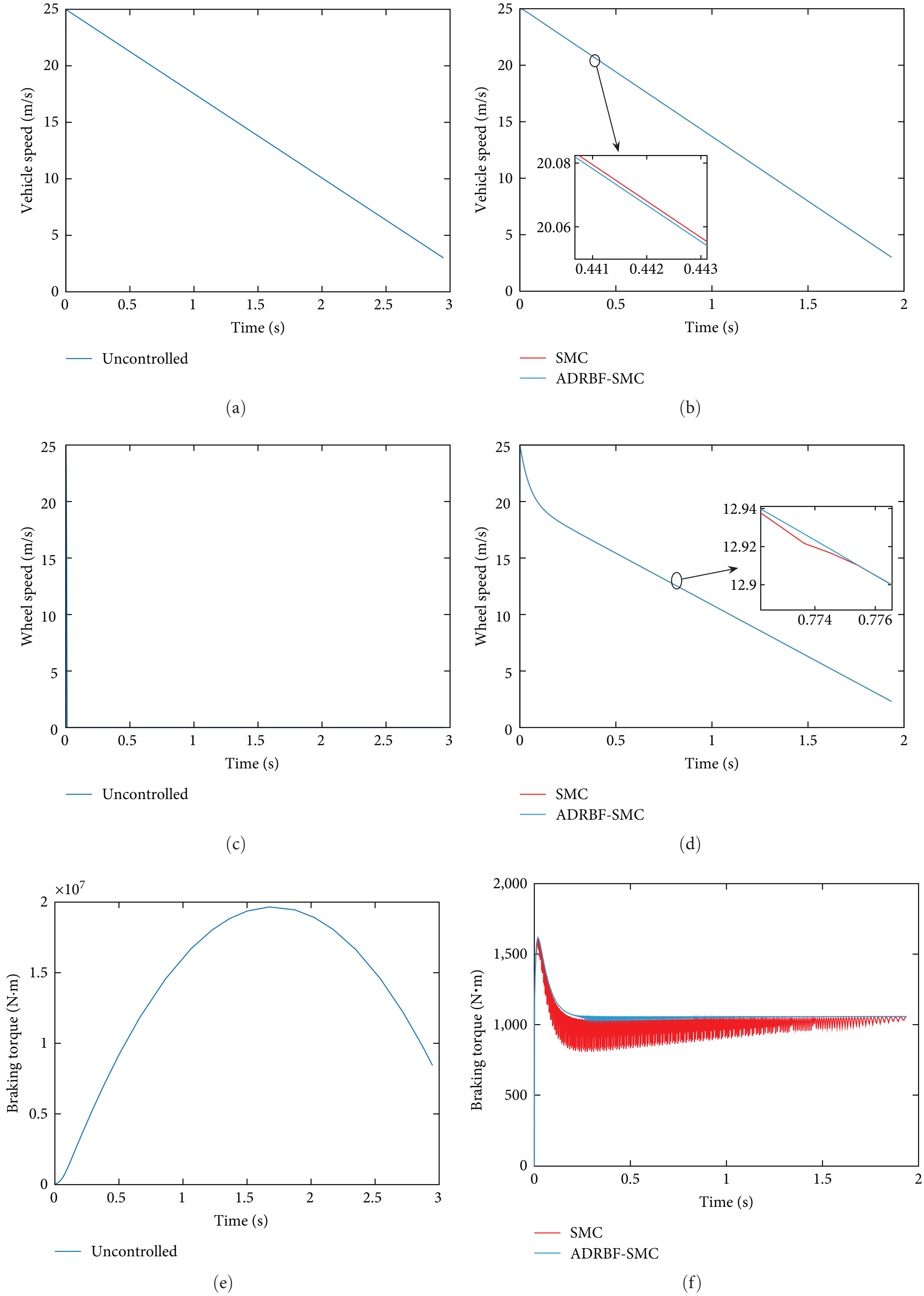

Figure 5: Continued.

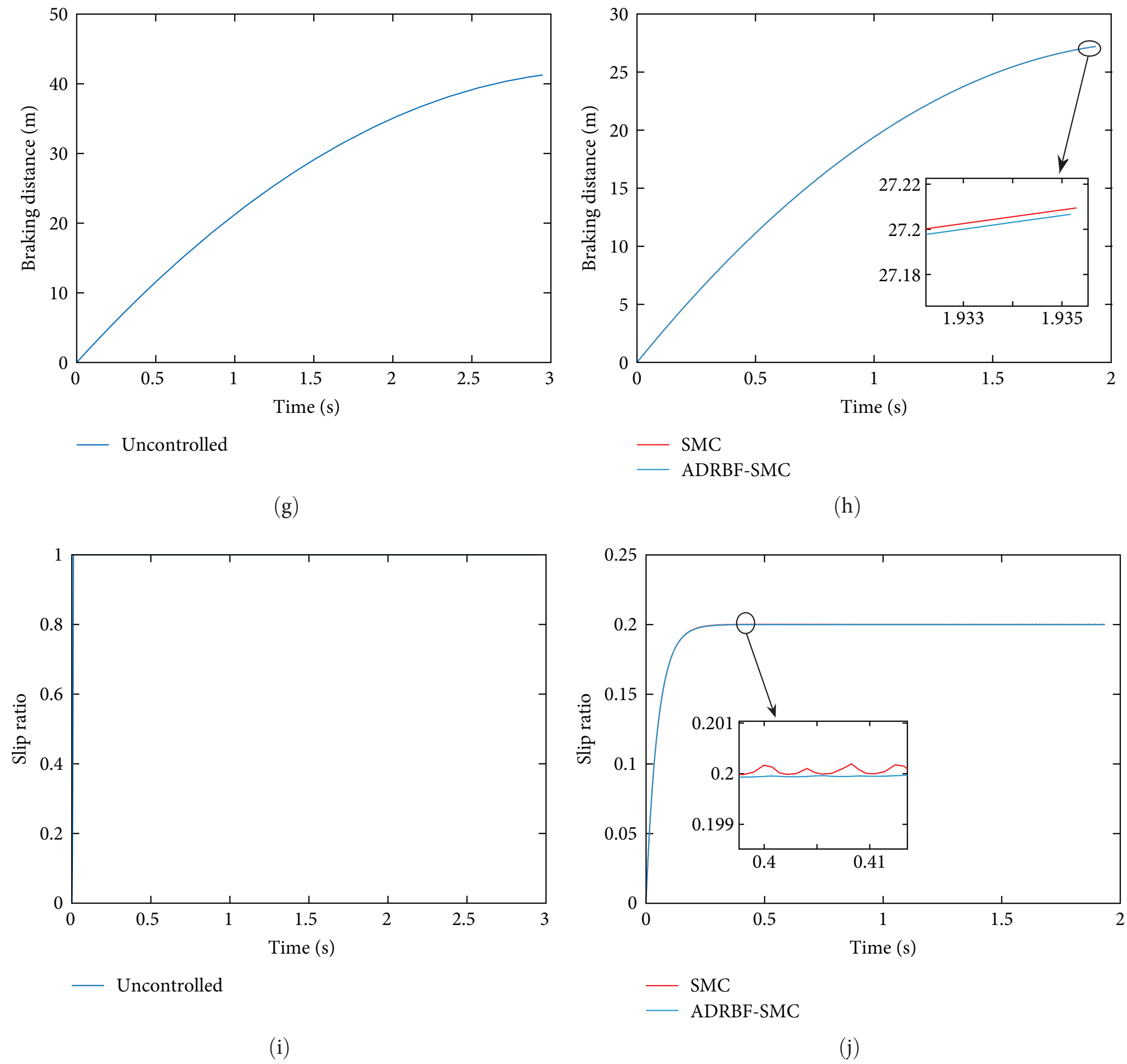

Figure 5: ABS vehicle quarter model simulations: (a) uncontrolled ABS speed; (b) SMC controlled ABS speed; (c) uncontrolled ABS wheel speed; (d) controlled ABS wheel speed; (e) uncontrolled ABS braking torque; (f) controlled ABS braking torque; (g) uncontrolled ABS braking distance; (h) controlled ABS braking distance; (i) uncontrolled ABS slip ratio; and (j) with controlled ABS slip ratio.

Table 2: Parametric simulation analysis results of ABS vehicle quarter model.

Description	Parameters	Units	Uncontrolled	SMC	ADRBF-SMC
Settling value	Time	s	2.9484	1.9351	1.9353
	Braking torque	$N\cdot m$	8,428,830	1,060.5287	1,058.0750
	Braking distance	m	41.2608	27.2095	27.2067
Buffet amplitude	Braking torque	—	—	226.562	22.65
	Slip ratio	—	—	0.000193	0.000017

The derivation of Equation (45) is obtained as follows:

$$\begin{aligned}\dot V_3 &= e\dot e + \gamma \widetilde{\boldsymbol{W}}^T \dot{\widehat{\boldsymbol{W}}} = -k_4 e^2 - \widetilde{\boldsymbol{W}}^T \boldsymbol{h}(\boldsymbol{x}) e + \theta\cdot e + \gamma \widetilde{\boldsymbol{W}}^T \dot{\widehat{\boldsymbol{W}}} \\ &= -k_4 e^2 + \widetilde{\boldsymbol{W}}^T\left(\gamma \dot{\widehat{\boldsymbol{W}}} - \boldsymbol{h}(\boldsymbol{x})e\right) + \theta e\end{aligned}. \tag{46}$$

To make $\dot V_3 \le 0$, design the adaptive rate as follows:

$$\dot{\widehat{\boldsymbol{W}}} = \frac{1}{\gamma}\boldsymbol{h}(\boldsymbol{x})e. \tag{47}$$

Associative Equations (46) and (47) are obtained as follows:

Table 3: Parameters of the full vehicle model for ABS vehicles.

Description	Symbol	Value	Units
Vehicle mass	m	1,220	kg
Height of CG	h	0.55	m
Distance from CG to front axle	a	1.18	m
Distance from CG to rear axle	b	1.29	m
coefficient of road adhesion	u	0.79	—
Front wheel tread	L_f	1.18	m
Rear wheel tread	L_r	1.29	m
Mass of single front wheel	m_f	98.1	kg
Mass of single rear wheel	m_r	79.7	kg
Front wheel angle	δ_{ij}	0	rad
windward area	A	1.8	m/s^2
Coefficient of air resistance	C_d	0.3	—
Air density	ρ	1.3	$N \cdot s^2 \cdot m^{-4}$
Coefficient of rolling resistance	f	0.015	—
The moment of inertia of the spring load mass	I_{xz}	21.09	$kg \cdot m^2$
Vehicle rotational inertia around z-axis	I_z	2,906	$kg \cdot m^2$
Wheel rolling radius	r	0.28	m
Wheel moment of inertia	I_w	3	$kg \cdot m^2$
Gravitational acceleration	g	9.8	m/s^2

$$\dot{V}_3 = -k_4 e^2 + \theta e \le -k_4 e^2 + \frac{1}{2} k_4 e^2 + \frac{1}{2} k_4 \theta^2 < -\frac{1}{2} k_4 e^2 + \frac{1}{2} k_4 \theta^{*2}, \tag{48}$$

where θ^* is a very small value, which is stable in the Lyapunov sense and there exists a domain of convergence.

The schematic diagram of the slip ratio control structure of adaptive neural network sliding mode controller (ADRBF-SMC) is shown in Figure 4.

4. Simulation and Analysis

The main research center of the article is about the slip ratio control problem in the ABS, aiming at demonstrating that the adaptive neural network sliding mode controller (ADRBF-SMC) proposed in the article is stronger robust and capable of solving the uncertainty problem in the ABS as compared to the sliding mode controller (SMC). MATLAB and Simulink software were used for model building and controller design. The main parameters are vehicle speed and wheel speed, braking torque, braking distance, and slip ratio in the quarter-vehicle model and the whole-vehicle model with no control as well as a comprehensive comparison analysis of the two control algorithms, respectively. The initial speed of the simulation is 25 m/s, and the simulation is stopped when the vehicle speed decelerates to 3 m/s. The main reason for this is when the speeds of the vehicle and wheels are near zero toward the end of braking, the slip ratio approaches infinity, and the simulation results are prone to jumping.

4.1. Vehicle Quarter Model Simulation Analysis. Table 1 shows the ABS vehicle quarter model parameters. No control, sliding mode control, and adaptive neural network sliding mode control for ABS slip ratio control on quarter-vehicle model, respectively, as shown in Figure 5. Table 2 shows the results of the parameter simulation analysis for the quarter model of the ABS vehicle. The table describes the numerical magnitude of the parameters and the magnitude of the jitter amplitude of the parameters when the simulation was stopped, with the jitter amplitude interpolated from the numerical change of the parameters over a shorter period of time. The jitter amplitude can reflect the anti-interference ability and robustness of the control algorithm.

Figure 5(a) shows the speed of the vehicle with no control. Figure 5(b) shows the vehicle speed under sliding mode control and adaptive neural network sliding mode control. The vehicles are in braking process and both show a linear decrease in speed, with the uncontrolled taking longer than the controlled vehicle. The SMC decreases the speed more slowly compared to the ADRBF-SMC. In real braking vehicle conditions, the lower the speed for the same time, the better.

Figure 5(c) shows the wheel speed with no control. Figure 5(d) shows the wheel speed under sliding mode control and adaptive neural network sliding mode control. In the vehicle without ABS control, during emergency braking, the wheels are held and the vehicle speed is zero because there is no limitation in the brake master cylinder pressure to control the braking torque. The wheel speed under ADRBF-SMC in Figure 5(d) is smoother as compared to the SMC, and it means it is easier to control.

Figure 5(e) shows the braking torque under no control. Figure 5(f) shows the braking torque under sliding mode control and adaptive neural network sliding mode control. The wheels are locked and the braking torque cannot be controlled, so the braking torque under no control is greatly and far more than the braking torque under control. Figure 5(f) and Table 2 show that the braking torque jitter

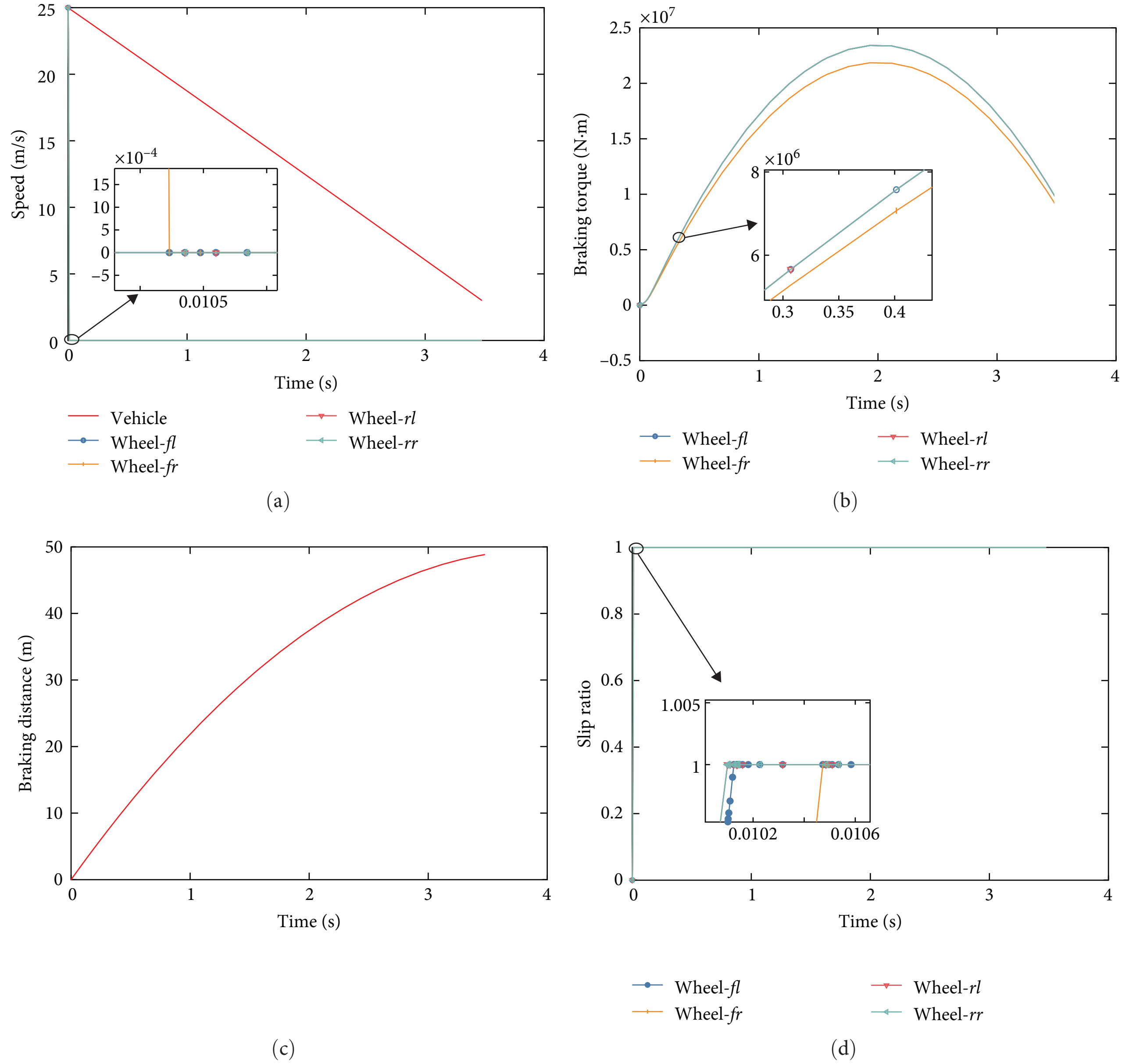

FIGURE 6: Full vehicle model uncontrolled simulation of ABS vehicle: (a) vehicle speed and wheel speed; (b) braking torque; (c) braking distance; and (d) slip ratio.

under SMC is intense, and the jitter amplitude is about 10 times of the ADRBF-SMC. The anti-interference ability and robustness of SMC are lower than that of ADRBF-SMC, which will affect the driving experience in the real road conditions.

Figure 5(g) shows the braking distance under no control. Figure 5(h) shows the braking distance under sliding mode control and adaptive neural network sliding mode control. The vehicle braking distance under no control ABS exceeds the vehicle braking distance under control ABS about 14 m. The difference between the vehicle braking distances under SMC and ADRBF-SMC in Figure 5(h) is small, and the braking distance under ADRBF-SMC is a little shorter.

Figure 5(i) shows the slip ratio under no control. Figure 5(j) shows the slip ratio under sliding mode control and adaptive neural network sliding mode control. The slip ratio under no control is 1, which reflects the wheel locking and the wheel are sliding during braking. Figure 5(j) and Table 2 show that the two control methods do achieve the slip ratio control objective, always tracking the ideal slip ratio. However, the tracking effect of ADRBF-SMC is better than that of SMC. The SMC jitter amplitude is about 11 times that of ADRBF-SMC.

4.2. Vehicle Whole-Vehicle Model Analysis Simulation. Table 3 shows the parameters of the whole vehicle model of the ABS vehicle. The uncontrolled ABS slip ratio on the vehicle whole-vehicle model is shown in Figure 6. Sliding mode controller (SMC) and adaptive neural network sliding mode controller (ADRBF-SMC) for ABS slip ratio control on vehicle whole-vehicle model, as shown in Figure 7. Table 4

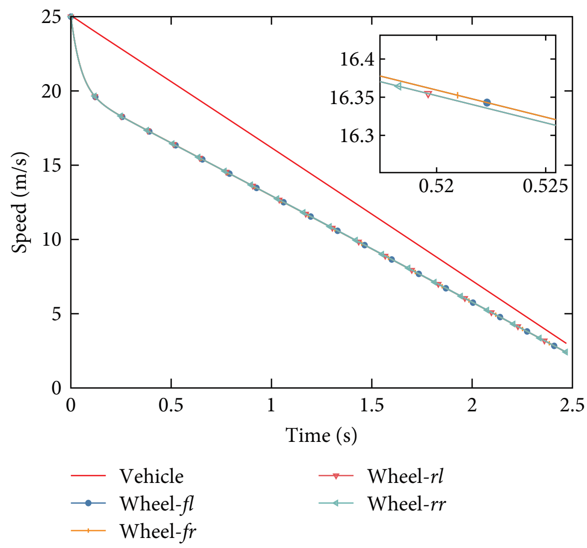

(a)

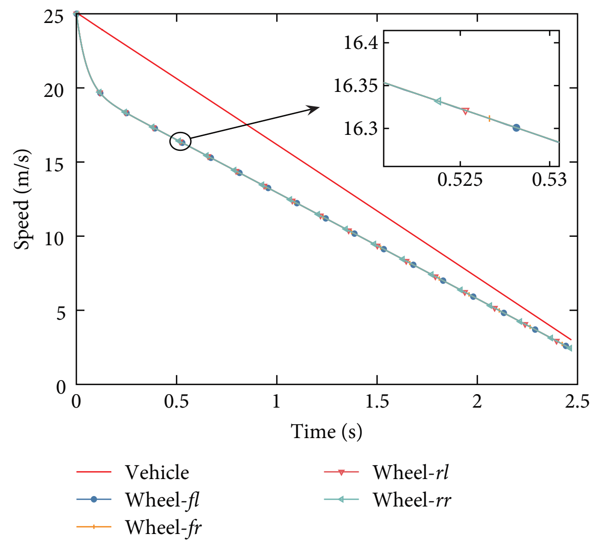

(b)

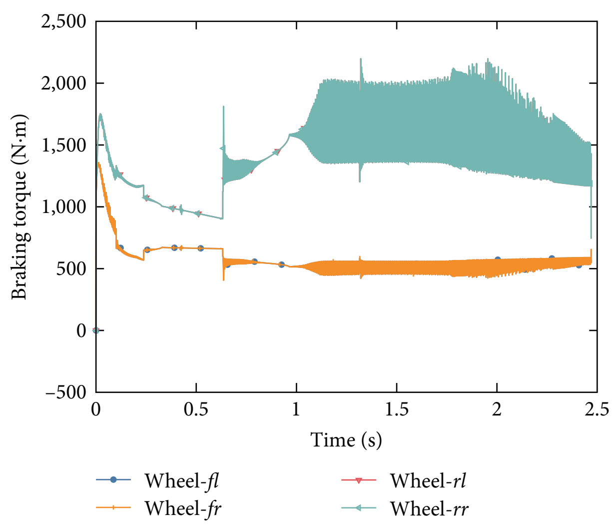

(c)

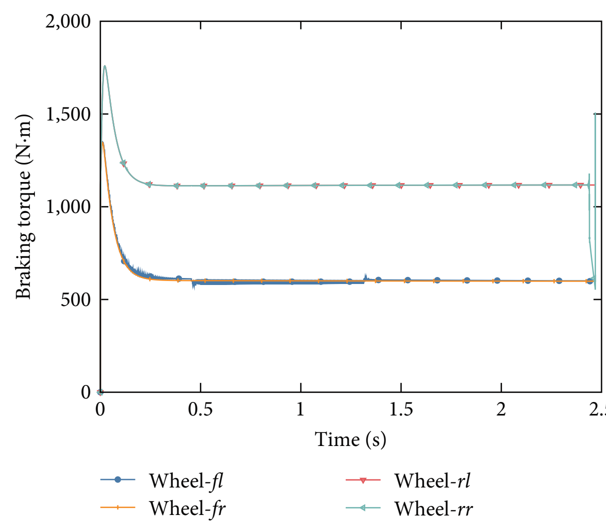

(d)

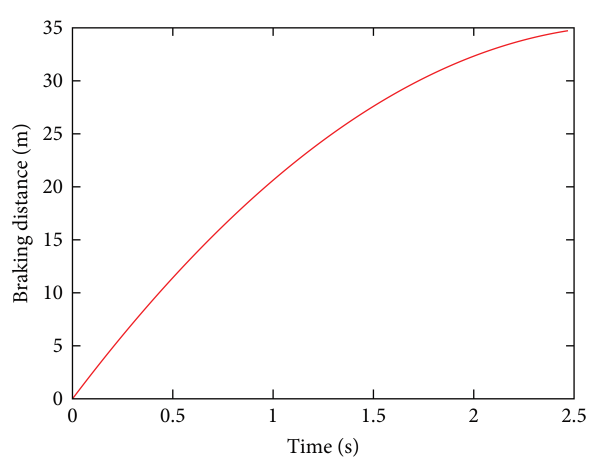

(e)

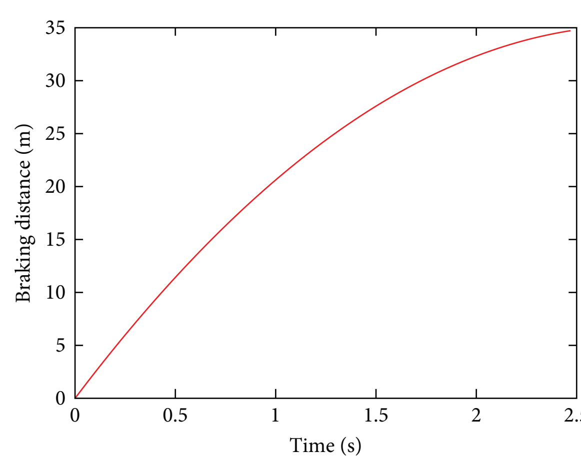

(f)

FIGURE 7: Continued.

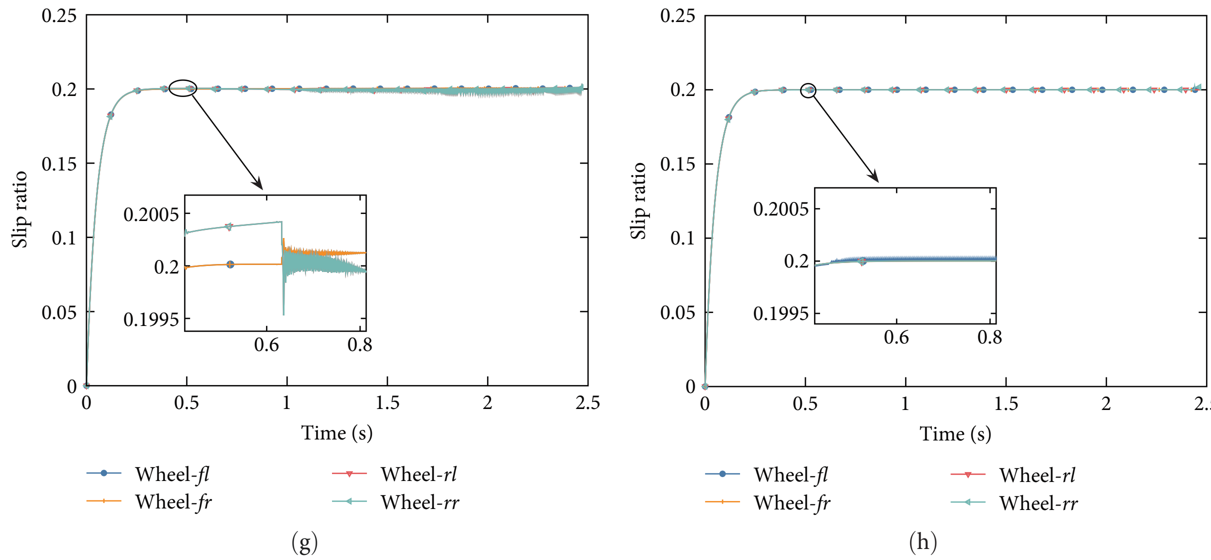

Figure 7: ABS whole-vehicle model uncontrolled simulation: (a) SMC vehicle speed and wheel speed; (b) ADRBF-SMC vehicle speed and wheel speed; (c) SMC braking torque; (d) ADRBF-SMC braking torque; (e) SMC braking distance; (f) ADRBF-SMC braking distance; (g) SMC slip ratio; and (h) ADRBF-SMC slip ratio.

Table 4: Parametric simulation analysis results of the full vehicle model of ABS vehicle.

Description	Parameters	Units	Uncontrolled	SMC	ADRBF-SMC
Settling value	Time	s	3.4770	2.4700	2.4690
	Left front wheel braking torque	N · m	9,967,856	659.2706	598.6706
	Right front wheel braking torque	N · m	9,303,373	659.2706	598.6198
	Left rear wheel braking torque	N · m	9,968,106	742.2228	1,117.432
	Right rear wheel braking torque	N · m	9,968,087	742.2228	1,117.163
	Braking distance	m	48.8480	34.7295	34.7225
Buffet amplitude	Left front wheel braking torque	N · m	—	142.64	20.148
	Right front wheel braking torque	N · m	—	142.64	0.008
	Left rear wheel braking torque	N · m	—	93.087	0.092
	Right rear wheel braking torque	N · m	—	93.087	0.078
	Left front wheel slip ratio	—	—	0.000371	0.00002
	Left rear wheel slip ratio	—	—	0.000371	0
	Right front wheel slip ratio	—	—	0.002260	0
	Right rear wheel slip ratio	—	—	0.002260	0

shows the results of the parametric simulation analysis of the ABS vehicle whole-vehicle model. The magnitude of the values of braking time, braking torque, and braking distance of four wheels and the magnitude of the jitter amplitude of braking torque of four wheels and slip ratio of four wheels at the time of stopping the simulation are demonstrated.

From Figure 6 and Table 4, it can be seen that the whole vehicle model with no control of ABS wheels holds the wheels at the beginning of braking, and after 3.5 s, the speed reaches 3 m/s and the braking distance is 48.84 m. The no control of the ABS makes the vehicle hold all four wheels and at this time, all four wheels behave with the same characteristics, but the data are no longer exactly the same. The right front wheel speed and braking torque of the vehicle deviated from the other three wheels, as shown in Figures 6(a) and 6(b). The two front wheel slip ratios and the two rear wheel slip ratios of the vehicle are different, as shown in Figure 6(d). The reason is that the vehicle whole-vehicle model is used more complex than the vehicle quarter model at this time, and there are more factors to consider, all of which influence the parameter indexes of each wheel.

Figures 7(a) and 7(b) show the vehicle speed and wheel speed under sliding mode control and adaptive neural network sliding mode control. According to the mathematical model, vehicle speed and wheel speed are the direct parameter indicators that influence the slip ratio. Under the same vehicle whole-vehicle model parameters, the vehicle and wheel speeds of both control methods can smoothly reduce, and there is a certain difference between the vehicle and wheel speeds, which can realize the proper slip ratio. In SMC, the two front wheel speeds and two rear wheel speeds are different because of the uncertainty of the vehicle model parameters. The whole vehicle model under ADRBF-SMC is also uncertain, but the speeds of the four wheels are basically the same, which shows that ADRBF-SMC is more robust compared to SMC.

Figures 7(c) and 7(d) represent the braking torque under sliding mode control and adaptive neural network sliding mode control, respectively. Braking torque is an indirect factor that affects the slip ratio, so the influence of wheel braking torque on the slip ratio is relatively small. As wheel braking torque acts as an actuator of ABS, a stable braking torque is more beneficial for ABS operation. In Figures 7(c) and 7(d), the shaking vibration amplitude of the braking torque under the sliding mode control is significantly larger than the adaptive neural sliding mode control. The braking torque of the ADRBF-SMC is more stable than the SMC braking torque, which is more efficient in suppressing the vibration.

Figures 7(e) and 7(f) represent the braking distances under sliding mode control and adaptive neural network sliding mode control, respectively. From Table 4, it can be seen that the braking distance of the vehicle under ADRBF-SMC is better than SMC. The main reason for this is that the proposed ADRBF-SMC on ABS control is more robust to SMC as well as more capable of resolving the uncertainty of the ABS.

Figures 7(g) and 7(h) represent the slip ratios under sliding mode control and adaptive neural network sliding mode control, respectively. The degree to which the slip rate converges to the ideal slip ratio reflects the efficiency of the control method. From Table 4, it can be seen that the slip ratio jitter amplitude of SMC is larger than that of ADRBF-SMC, indicating that the robustness of ADRBF-SMC is better.

5. Conclusion

In this paper, to solve the problems of nonlinearity, time-varying, and parameter model uncertainty faced by ABS, adaptive neural network sliding mode controller (ADRBF-SMC) is proposed on the basis of sliding mode controller (SMC), and the following conclusions can be obtained:

(1) Both the proposed ADRBF-SMC and SMC effectively control the realized ABS slip ratio in the developed vehicle quarter model and vehicle whole vehicle model. ADRBF-SMC and SMC-based ABS controllers achieve shorter braking times and shorter braking distances than uncontrolled braking.

(2) The proposed ADRBF-SMC and SMC still achieve the control of ABS slip ratio for the model uncertainty which exists in the quarter-vehicle model and seven-degree-of-freedom vehicle model.

(3) In the vehicle quarter model, the jitter amplitude of the braking torque of the SMC is about 10 times that of the ADRBF-SMC. The slip ratio jitter amplitude of the SMC is about 11 times that of the ADRBF-SMC. In the whole-vehicle model of the vehicle, the braking torque and slip ratio jitter amplitude of ADRBF-SMC are smaller compared to those of SMC control. The proposed ADRBF-SMC is more robust than SMC.

Data Availability

The data used to support the findings of this study are included within the article.

Conflicts of Interest

The authors declare that they have no conflicts of interest.

References

[1] A. O. Moaaz, A. S. Ali, and N. M. Ghazaly, "Investigation of anti-lock braking system performance using different control systems," *International Journal of Control and Automation*, vol. 13, no. 1s, pp. 137–153, 2020.

[2] Z. He, Q. Shi, Y. Wei, B. Gao, B. Zhu, and L. He, "A model predictive control approach with slip ratio estimation for electric motor antilock braking of battery electric vehicle," *IEEE Transactions on Industrial Electronics*, vol. 69, no. 9, pp. 9225–9234, 2022.

[3] W. Li, Q. Zhang, and Y. Zhang, "The effect of ADRC on vehicle braking performance," *Journal of Electrical Engineering & Technology*, vol. 15, pp. 705–712, 2020.

[4] D. Wang, S. Liu, X. Wei, and Y. He, "A wheel slip ratio constraint control for ABS based on tangent type barrier Lyapunov function," *Measurement and Control*, vol. 56, no. 1-2, pp. 411–419, 2023.

[5] H. Wang, S. Wu, and Q. Wang, "Global sliding mode control for nonlinear vehicle antilock braking system," *IEEE Access*, vol. 9, pp. 40349–40359, 2021.

[6] C. J. García Torres, L. A. Ferré Covantes, C. C. Vaca García, J. C. Estrada Gutiérrez, A. N. Guzmán, and C. Acosta Lúa, "A Lyapunov stability analysis of modified HOSM controllers using a PID-sliding surface applied to an ABS laboratory setup," *Applied Sciences*, vol. 12, no. 8, Article ID 3796, 2022.

[7] Z. Zhang, R. Ma, L. Wang, and J. Zhang, "Novel PMSM control for anti-lock braking considering transmission properties of the electric vehicle," *IEEE Transactions on Vehicular Technology*, vol. 67, no. 11, pp. 10378–10386, 2018.

[8] X. Feng and J. Hu, "Discrete fuzzy adaptive PID control algorithm for automotive anti-lock braking system," *Journal of Ambient Intelligence and Humanized Computing*, pp. 1–10, 2021.

[9] A. Amirkhani, M. Shirzadeh, and M. Molaie, "An indirect type-2 fuzzy neural network optimized by the grasshopper algorithm for vehicle ABS controller," *IEEE Access*, vol. 10, pp. 58736–58751, 2022.

[10] A. Shahabi, A. H. Kazemian, S. Farahat, and F. Sarhaddi, "Wheel slip ratio regulation for investigating the vehicle's dynamic behavior during braking and steering input," *Mechanics & Industry*, vol. 22, Article ID 17, 2021.

[11] J. Zhang, Z. Shi, X. Yang, and J. Zhao, "Robust adaptive control for continuous wheel slip rate tracking of vehicle with state observer," *Measurement and Control*, vol. 53, no. 7-8, pp. 1331–1341, 2020.

[12] H. Ben Moussa and M. Bakhti, "Robustness analysis for adaptive model predictive and sliding mode controllers regulating longitudinal tire slip ratio," *IFAC-PapersOnLine*, vol. 55, no. 12, pp. 586–591, 2022.

[13] J. Zhang, S. Zhou, and J. Zhao, "Nonlinear robust wheel slip rate tracking control for autonomous vehicle with actuator dynamics," *Advances in Mechanical Engineering*, vol. 12, no. 6, 2020.

[14] C.-F. Hsu, "Intelligent exponential sliding-mode control with uncertainty estimator for antilock braking systems," *Neural Computing and Applications*, vol. 27, pp. 1463–1475, 2016.

[15] E. Chereji, M.-B. Radac, and A.-I. Szedlak-Stinean, "Sliding mode control algorithms for anti-lock braking systems with performance comparisons," *Algorithms*, vol. 14, no. 1, Article ID 2, 2021.

[16] M.-B. Radac and R.-E. Precup, "Data-driven model-free slip control of anti-lock braking systems using reinforcement Q-learning," *Neurocomputing*, vol. 275, pp. 317–329, 2018.

[17] J.-C. Wang and R. He, "Hydraulic anti-lock braking control strategy of a vehicle based on a modified optimal sliding mode control method," *Proceedings of the Institution of Mechanical Engineers, Part D: Journal of Automobile Engineering*, vol. 233, no. 12, pp. 3185–3198, 2019.

[18] L. Lv, J. Wang, and J. Long, "Interval type-2 fuzzy logic anti-lock braking control for electric vehicles under complex road conditions," *Sustainability*, vol. 13, no. 20, Article ID 11531, 2021.

[19] Q. Fu, "Research on fuzzy control method of automobile antilock braking system," *Security and Communication Networks*, vol. 2022, Article ID 5001185, 9 pages, 2022.

[20] J. Sun, X. Xue, and K. W. E. Cheng, "Four-wheel anti-lock braking system with robust adaptation under complex road conditions," *IEEE Transactions on Vehicular Technology*, vol. 70, no. 1, pp. 292–302, 2021.

[21] D. Yu, W. Wang, H. Zhang, and D. Xu, "Research on anti-lock braking control strategy of distributed-driven electric vehicle," *IEEE Access*, vol. 8, pp. 162467–162478, 2020.

[22] L. He, W. Ye, Z. He, K. Song, and Q. Shi, "A combining sliding mode control approach for electric motor anti-lock braking system of battery electric vehicle," *Control Engineering Practice*, vol. 102, Article ID 104520, 2020.

[23] A. Soltani, S. Azadi, and R. N. Jazar, "Integrated control of braking and steering systems to improve vehicle stability based on optimal wheel slip ratio estimation," *Journal of the Brazilian Society of Mechanical Sciences and Engineering*, vol. 44, Article ID 102, 2022.

[24] J. Sun, X. Xue, and K. W. E. Cheng, "Fuzzy sliding mode wheel slip ratio control for smart vehicle anti-lock braking system," *Energies*, vol. 12, no. 13, Article ID 2501, 2019.

[25] S. Zhu, X. Fan, G. Qi, and P. Wang, "Review of control algorithms of vehicle anti-lock braking system," *Recent Patents on Engineering*, vol. 17, no. 2, pp. 30–45, 2023.

[26] M. Burckhardt, *Fahrwerktechnik: Radschlupf-Regelsysteme*, Vogel Fachbuch, Würzburg, Germany, 1993.

[27] A. Bagheri, S. Azadi, and A. Soltani, "A combined use of adaptive sliding mode control and unscented Kalman filter estimator to improve vehicle yaw stability," *Proceedings of the Institution of Mechanical Engineers, Part K: Journal of Multi-body Dynamics*, vol. 231, no. 2, pp. 388–401, 2017.

[28] S. Meng, F. Meng, F. Zhang, Q. Li, Y. Zhang, and A. Zemouche, "Observer design method for nonlinear generalized systems with nonlinear algebraic constraints with applications," *Automatica*, vol. 162, Article ID 111512, 2024.

[29] H. Mirzaeinejad and M. Mirzaei, "A novel method for non-linear control of wheel slip in anti-lock braking systems," *Control Engineering Practice*, vol. 18, no. 8, pp. 918–926, 2010.

[30] J. Park and I. W. Sandberg, "Universal approximation using radial-basis-function networks," *Neural Computation*, vol. 3, no. 2, pp. 246–257, 1991.

[31] B. Tutmez, "Assessment of porosity using spatial correlation-based radial basis function and neuro-fuzzy inference system," *Neural Computing and Applications*, vol. 19, pp. 499–505, 2010.